iScience

CellPress
OPEN ACCESS

Article

Strongly plasticized gelatin-based hydrogel for flexible encapsulation of complex-shaped electronic devices

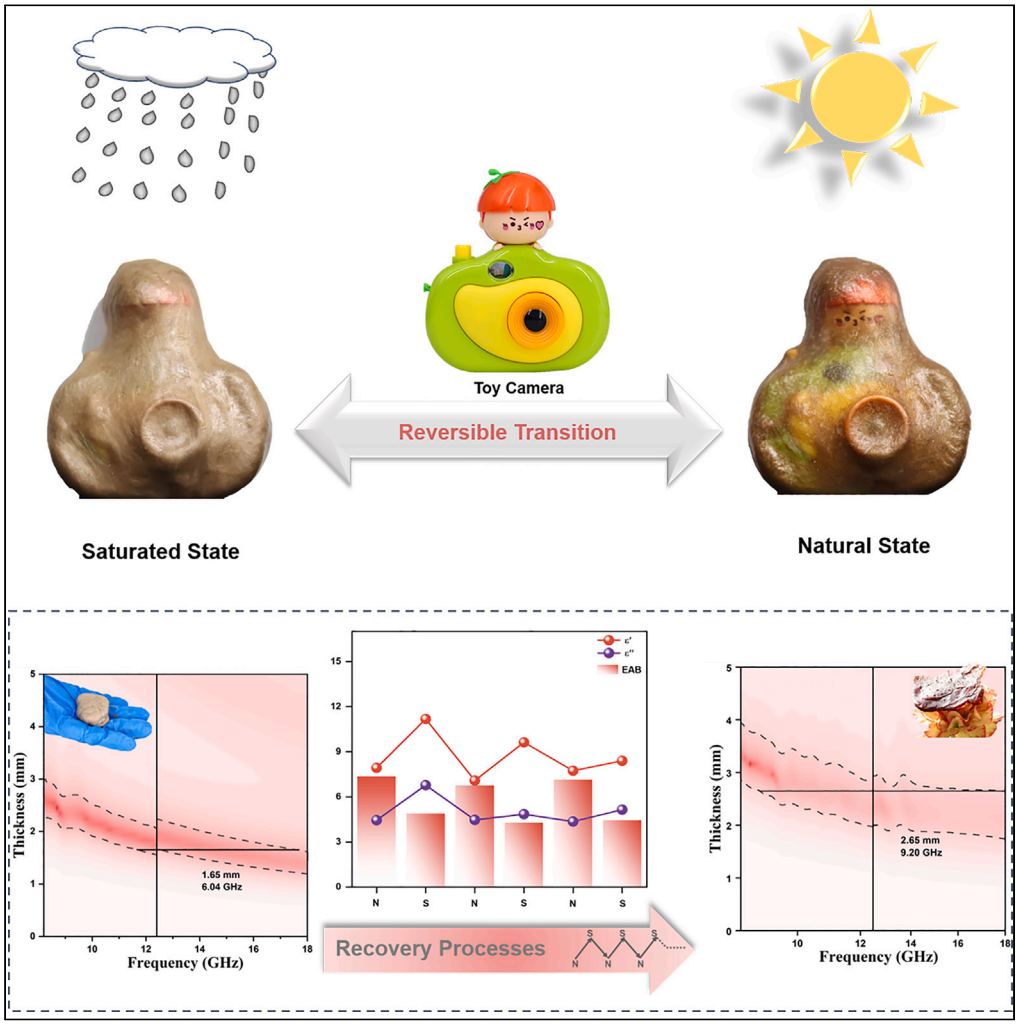

Xinyu Zhang, Yuntong Wang, Bin Shi, Dongwei Bi, Qing Chang, Limin Zhang, Hongjing Wu

changqingyau@126.com (Q.C.)
wuhongjing@nwpu.edu.cn (H.W.)

Highlights

Water loss property of gels was utilized for flexible encapsulation of ECEDs

Self-optimization of EMW absorption was achieved after water loss process of gels

Ultrawide EMW absorption were obtained in NGT (EAB_{NGT} = 9.20 GHz)

Zhang et al., iScience 27, 109725
May 17, 2024
https://doi.org/10.1016/j.isci.2024.109725

iScience

CellPress
OPEN ACCESS

Article

Strongly plasticized gelatin-based hydrogel for flexible encapsulation of complex-shaped electronic devices

Xinyu Zhang,[1] Yuntong Wang,[1] Bin Shi,[1,2] Dongwei Bi,[1] Qing Chang,[1,2,*] Limin Zhang,[1] and Hongjing Wu[1,3,*]

SUMMARY

The growth of environmentally sensitive complex-shaped electronic devices (ECEDs) has led to a surging demand for flexible electromagnetic wave (EMW) absorbers. Herein, the water loss property of hydrogel was ingeniously applied for the flexible encapsulation (FE) of ECEDs. To be specific, saturated state (SGT) hydrogels were prepared by chemical cross-linking, and the hydrogen bond dissipation network promoted FE. Additionally, SGT has an effective absorption bandwidth (EAB) of 6.04 GHz at 1.65 mm due to the presence of dipole polarization. With the loss of water, SGT transitions to its natural state (NGT), and the decreasing conductivity leads to better impedance matching. NGT exhibited a broader EAB (9.20 GHz at 2.65 mm) and also strength and lightness (density of 0.3 g cm^{-3}). Furthermore, the semi-automatic reversible cyclic transformation between SGT and NGT gels further broadens application scenarios. GT gel combines self-encapsulation and self-optimized performance as a potential EMW absorber for FE.

INTRODUCTION

The progression of innovations like bionic robotics and diverse-shaped precision electronic instrumentation demands forthcoming electromagnetic wave (EMW) absorbers to exhibit multifaceted applicability and multifunctional capabilities.[1–3] Environmentally sensitive, wear-prone, and complex-shaped electronic devices (ECEDs) are susceptible to external factors such as impact and weather, especially the interface between device components, and thus the overall packaging of the EMW absorption layer is urgent and important.[4,5] Fortunately, flexible encapsulation (FE) enables comprehensive sealing, effectively eliminating radiation gaps and achieving efficient EM protection for the ECEDs.[6]

Gel-type materials are highly deformable to help realize FE. Specifically, realizing impeccable FE demands materials with outstanding mechanical properties, particularly flexibility and plasticity.[7,8] Most gel materials contain hydrogen bonds with reversible dissipative networks that modulate their mechanical properties,[9] and gels are three-dimensional (3D) cross-linked polymer networks that retain a large amount of liquid without defects or vacancies, overcoming the shortcomings of uncontrollable absorption performance of conventional absorbent and facilitating mass production.[10,11] For example, Xue et al. synthesized hydrogels with high conductivity, strain sensitivity, wide strain range, and high stability after more than 300 loading-unloading cycles at 100% strain by *in situ* co-polymerization.[8] Long et al. prepared hematite (Fe_2O_3) @carbon nanotubes (CNTs)/polyacrylamide hydrogel composites with good flexibility and biocompatibility, with RL_{min} of −60.96 dB at 15.87 GHz and an effective absorption bandwidth (EAB) of about 3.4 GHz.[12] However, hydrogel-type EMW absorbers exhibit poor durability, due to the decreasing polar water molecular leads to the decline or even disappearance of the polarization phenomenon, which results in an impact on the electromagnetic wave absorption (EWA) performance, limiting its practical application.[13,14]

Herein, we ingeniously leveraged the inherent water loss property of conventional hydrogels to achieve the flexible integrated encapsulation of complex-shaped devices. Specifically, gelatin-based (GT) hydrogels, namely saturated state (SGT), were prepared through a chemical cross-linking method, and the exceptional flexibility and plasticity provided by the "soft" hydrogen bonding in SGT gel facilitates the encapsulation of the ECEDs in the initial phases.[15,16] With the loss of water, the 'soft' hydrogen bonding in SGT changes to 'hard' covalent bonding in its natural state (NGT), and the "hard" covalent bonding in NGT drives lightweight (density of 0.3 g cm^{-3}) and strong materials, conducive to realizing the encapsulation protection for environmentally sensitive ECEDs.[17–19] Surprisingly, the NGT gel exhibited an ultrawide effective absorption bandwidth (EAB) of 9.20 GHz at 2.65 mm and a minimum reflection loss (RL_{min}) of −54.2 dB, far exceeding the performance in SGT gel (EAB = 6.04 GHz at 1.65 mm) due to the reduction of hydrogen bonding which leads to a decrease in the electrical conductivity, resulting in a better impedance matching. Further, it was verified that SGT and NGT gels are expected to achieve semi-automated reversible cyclic transformations in different scenarios, which further widens the scenarios of the gels. This work introduces an innovative

[1]MOE Key Laboratory of Material Physics and Chemistry under Extraordinary, School of Physical Science and Technology, Northwestern Polytechnical University, Xi'an, Shaanxi 710072, China
[2]College of Chemistry and Chemical Engineering, Shaanxi Key Laboratory of Chemical Reaction Engineering, Yan'an University, Yan'an, Shaanxi 716000, China
[3]Lead contact
*Correspondence: changqingyau@126.com (Q.C.), wuhongjing@nwpu.edu.cn (H.W.)
https://doi.org/10.1016/j.isci.2024.109725

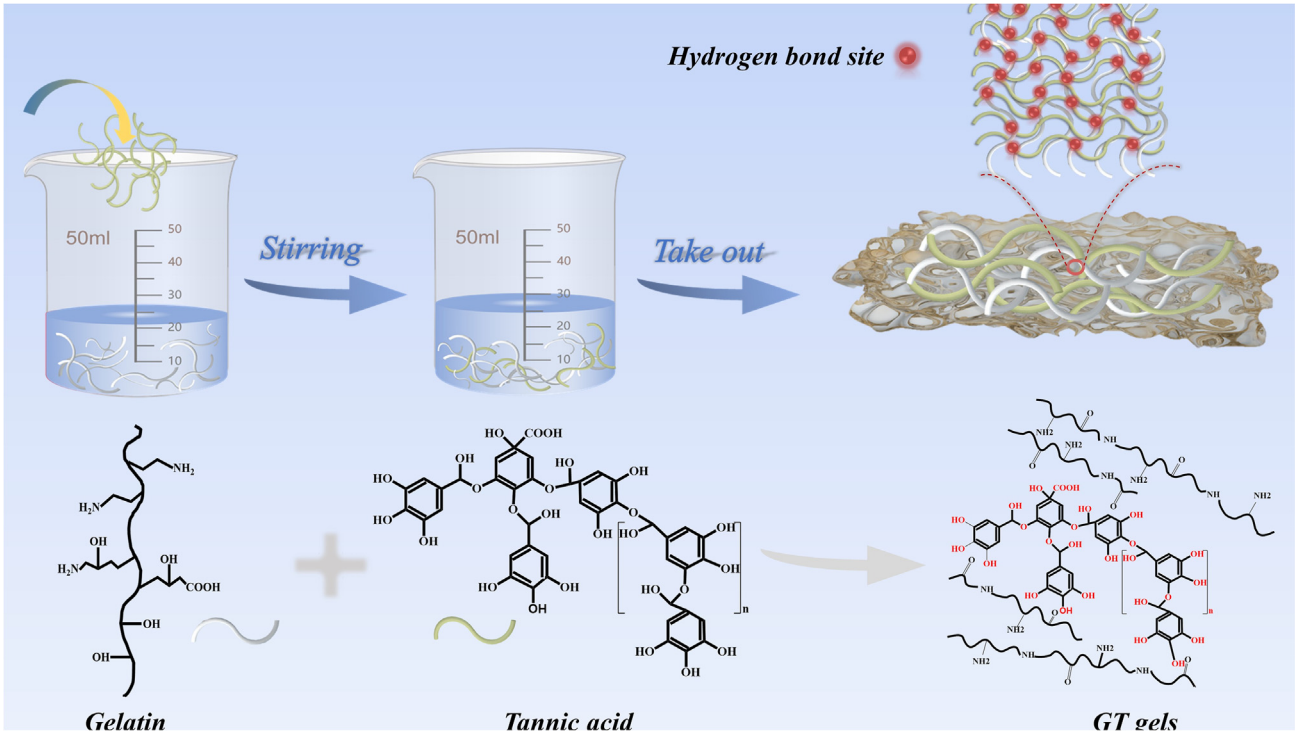

Figure 1. Schematic preparation of SGT gels

strategy for designing EWA gels that exploits the characteristics of traditional hydrogel materials to address their application. Furthermore, the process of GT gels is low-cost, raw materials are readily available and can be rapidly prepared in 5 min. It is expected to be applied to the protection of ECEDs.

RESULTS AND DISCUSSION

Synthesis of SGT gels and EM loss mechanism

Figure 1 illustrates the preparation process of GT gels. Gelatin, a hydrolyzed product of collagen, when heated above the gelation temperature, the triple-helical structure dissociates into a single chain, it is easy to modify, thus proving to be an exceptional candidate for constructing polymer networks.[20–22] Moreover, tannic acid possesses polyphenolic hydroxyl structures that foster numerous hydrogen-bonding interactions, facilitating the establishment of intricate 3D networks within GT gel and imparting distinctive hydrophobic characteristics. The phenolic hydroxyl group present in tannic acid undergoes a chemical reaction with -NH_2 within gelatin, resulting in the creation of cross-linking structures (-COO or -NH-) that establish durable covalent bonds, ensuring the structural stability of GT gels.[23,24] Through a singular one-step amalgamation involving gelatin and tannic acid solutions, the SGT gel is obtained. The synthesis of SGT gels utilized cost-effective raw materials and a straightforward, rapid chemical cross-linking method, which addresses the drawbacks associated with the high cost and complex processes involved in traditional gel preparation.

To explore intermolecular interactions within the polymer network, we conducted a detailed analysis of the chemical composition of GT gels using FTIR (Figure 2A). The broad band at 3308 cm^{-1} is attributed to the O-H or N-H stretching vibrations, while the peaks at 1714 cm^{-1} and 1624 cm^{-1} are caused by the stretching vibrations of C=O-O and C=O bonds. In addition, the difference between GT gel and tannic acid FTIR spectra was represented by a redshift peak from 3361 cm^{-1} to 3308 cm^{-1}, corresponding to the stretching vibration of -OH, these results indicate that tannic acid was successfully crosslinked with gelatin through hydrogen bonding.[25,26] Remarkably, all GT gels with different mass ratios had the same FTIR spectra, indicating that variations in tannic acid content cause no change in the composition and chemical structure of the gels.[27,28] We also characterized the functional groups of the gel with XPS spectra (Figures 2B and 2C). In the $O1_S$ spectrum, two characteristic peaks at 529.8 eV and 528.5 eV signify C-O and C=O, respectively. Similarly, the $N1_S$ spectrum exhibits two characteristic peaks at 398.3 eV and 396.4 eV, corresponding to -NH- and -NH_2, aligning with the findings from IR spectroscopy.[29,30] In summary, the numerous polar functional groups existing in SGT gels can act as dipoles to dissipate EMW energy through polarization loss.

The thermal stability of SGT gels was assessed via thermogravimetric analysis (TGA) in the temperature range of 30°C–250°C (Figure 2D). A comparison of thermal stability among SGT gels with different mass ratios revealed the following pattern: SGT-1.0<SGT-0.8<SGT-1.6<SGT-1.2<SGT-1.4<SGT-0.6. Among these, SGT-1.6 exhibits excellent thermal stability, losing only 9.0% of its initial mass loss at 100°C, attributed to extensive hydrogen bonding interactions within the polymer network. Despite a decline in thermal stability with the increasing temperature

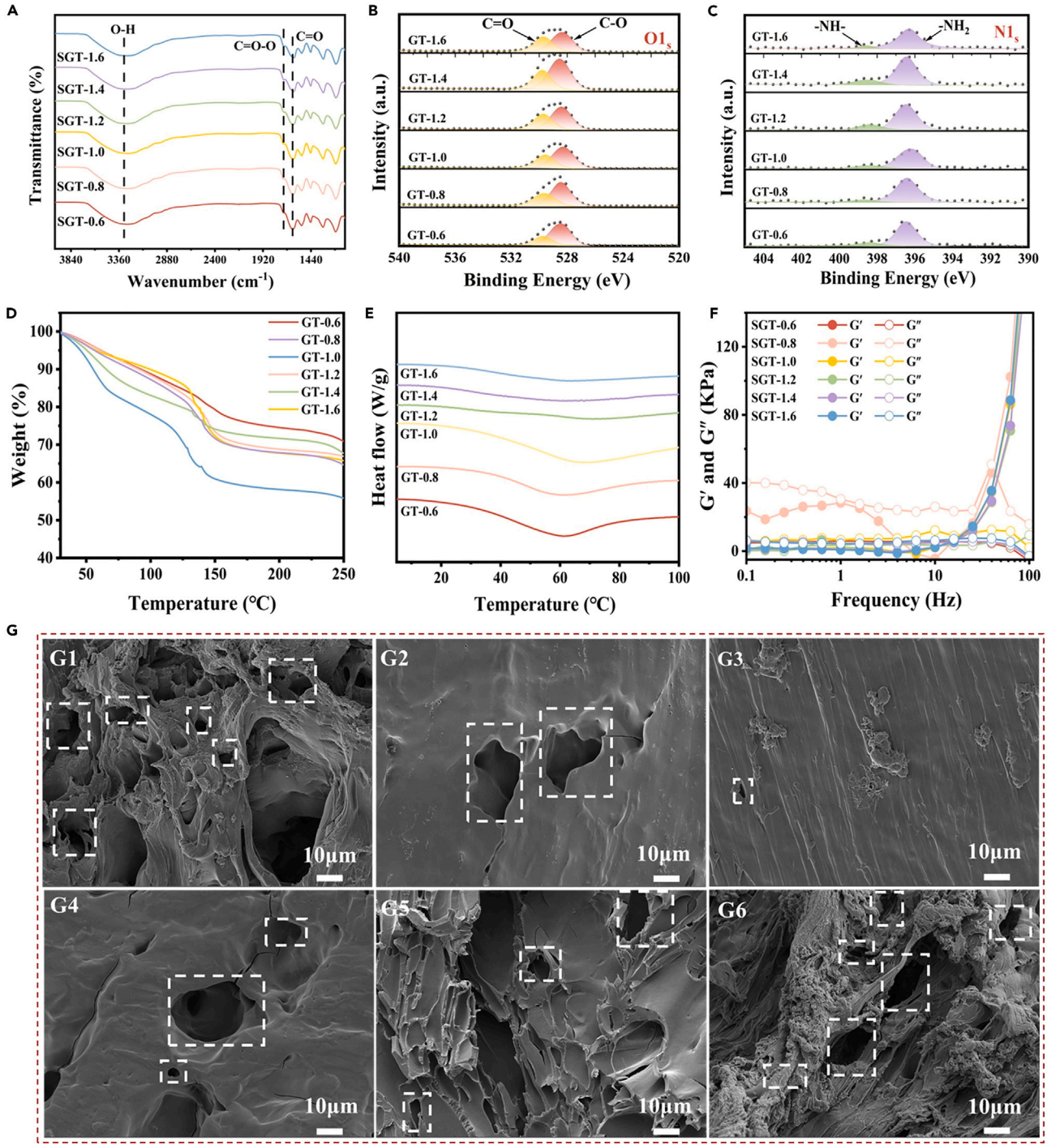

Figure 2. Morphology and structure characterizations of SGT gels

(A) FTIR spectrum of SGT gels.

(B and C) XPS spectra of O1s and N1s.

(D) TGA characterizations of SGT gels.

(E) DSC characterizations of SGT gels.

(F) Rheological characterizations of SGT gels.

(G) SEM images of GT gels.

due to the breaking of hydrogen bonds, SGT-0.6 retains 70% of its mass even at a high temperature of 200°C, substantiating the prominent thermal stability of SGT gels and their suitability for high-temperature environments.[31,32] Further, the thermal properties of the gels were tested using Differential Scanning Calorimetry (DSC) in the temperature range of 5°C–100°C (Figure 2E). No crystallization peaks appeared throughout the temperature interval of 5°C/min, revealing the amorphous nature of GT gels. Meanwhile, the DSC curves showed linear distributions over a wider temperature range above 5°C, with no tendency toward glass transition or phase change, indicating that the mechanical properties of GT gels remain essentially unchanged over the temperature range.[33,34]

Rheological tests at different frequencies were performed on SGT gels to investigate the viscoelastic characteristics of SGT gels (Figure 2F). No intersection occurs between the storage modulus (G′) and loss modulus (G′′) of the SGT gels, affirming the accomplished transition from the sol to the gel state. the G′ of the SGT gel consistently remains inferior to G″, confirming its viscous nature and suggesting adhesive properties in the SGT gel.[35,36] The cross-sectional morphology of a series of lyophilized gels underwent examination using Scanning Electron Microscopy (SEM), with SEM images further confirming the amorphous nature of the gels. In addition, the porous internal structure evidences the abundant water content in the SGT gels, and the presence of water ensures electron movement in the hydrogel, thus improving the electrical conductivity (Figure 2G).

To verify the EWA performance of the gels across the 8.2–18 GHz, the dielectric properties of all gels were assessed through EM parameters, including complex permittivity (ε' and ε'') as well as complex relative permeability (μ' and μ''). It is noteworthy that all gels demonstrate non-magnetic properties, resulting in a negligible complex permeability. The EM parameters and EAB of samples with diverse compositional ratios are presented in Figures 3A and S1. Discrepancies in dipole and conduction loss levels within the SGT gel samples contribute to variations in EM parameters and EAB performance. The patterns of change in dielectric and EAB for a series of SGT gels are respectively shown in Figures 3B and 3C. The dielectric constant exhibits a trend of initially increasing and then decreasing. As shown in Figures 3D and S2, the *Cole-Cole* curves with different mass ratios exhibit distinct semicircles, indicating the presence of polarization behavior. The dipoles engage in polarization and relaxation processes when exposed to a dynamic EM field, effectively dissipating EM energy.[37–39] To further demonstrate the existence of dipole polarization, we utilized the computational framework of Density Functional Theory (DFT) (Figure 3E). Calculations of charge density differences reveal that various polar functional groups in the molecule generate positive and negative charges. Differences in electronegativity lead to the generation of dipoles within these charge centers.[40] Specifically, through hydrogen bonding, -OH in tannic acid interacts with -NH_2 in gelatin, allowing electrons to be transferred between the different groups so that dipole polarization occurs under the action of an alternating EM field. The introduction of tannic acid containing massive polar functional groups causes enhanced dipole polarization. The impedance profile of the SGT gel is shown in Figure S3, which is consistent with the performance.

Moreover, the non-covalent bonding of tannic acid to proteins is reversible, and their interaction is influenced by solution pH.[41–43] When gelatin reacts with tannic acid, each -OH in tannic acid reacts with one -NH_2 of gelatins, and at a mass ratio of 1:1 the tannic acid reacts sufficiently with the gelatin to form a combination of non-covalent bonds in the polymer network (GT-1.0). The presence of hydrogen bonding contributed to the electrical conductivity.[44,45] Hence, from SGT-0.6 to SGT-1.0, the complex dielectric constant tends to increase as the hydrogen bonding between the polymer networks enhances the electrical conductivity, and the dielectric constant is proportional to the electrical conductivity. The high ε' of SGT-1.0 leads to impedance mismatch, which produces the worst EAB. Thereafter, the continuous addition of tannic acid decreased the solution pH, weakening the hydrogen bonding, and the conductivity gradually decreased, so the complex permittivity of the samples from SGT-1.0 to SGT-1.6 shows a decreasing trend. SGT-1.6 has the best impedance match ($|Z| = 0.75$) and exhibits favorable EWA performance.

Microscopic mechanism and EW loss mechanism of SGT to NGT transition

The NGT can be obtained by drying SGT in a natural state, exhibiting characteristics of lightness and stability. To investigate the viscoelastic characteristics of GT gels in various states, rheological tests were also conducted at varying frequencies for NGT. As depicted in Figure 4A, with the lack of water, a significant fraction -OH functional groups break, and the decrease of hydrogen bonds leads to the formation of stronger covalent cross-links between tannins and gelatin. The rheological profile of NGT gels exhibits a distinctive jagged pattern, signifying that the transition from SGT to NGT induces a shift in the dynamics within the gel polymer network.[46] In a word, there is a transition from a dominance of hydrogen bonding to a prevalence of covalent bonding in the GT gel structure.

To investigate the transformation mechanism from SGT to NGT, we assessed the EM parameters and impedance matching of NGT gels (Figures 4B, S4, and S5). Notably, the impedance matching of a series of NGT gels was significantly higher than that of SGT gels ($|Z| = 0.79$). The complex permittivity of NGT-1.6 decreases significantly compared with that of SGT-1.6, and the EAB of NGT-1.6 can reach 9. 20 GHz at a thickness of 2.65 mm. During the transition between SGT and NGT, the complex dielectric constant decreases for two reasons: firstly, hydrogen bonding in the polymer network has the role of transporting electrons.[17] The dominant bonding changes from hydrogen to covalent bonding, and the reduction of hydrogen bonding hinders electron transport, leading to a decrease in conductivity and resulting in a better impedance match. Secondly, with large losses of highly dielectric water in NGT, the bonding between polymer chains is dominated by tight covalent bonds. The assessment of EWA performance commonly relies on metrics such as reflection loss (RL) and EAB. The RL_{min} for SGT-1.6 was calculated to be −35.8 dB, and NGT-1.6 exhibited an RL_{min} of −54.2 dB (Figure 4C), showcasing the self-optimization of EWA performance. A plot illustrating the relationship between RL and thickness for NGT-1.6 is presented in Figure S6.

It is surprising that the GT gel not only has self-optimized EWA performance but also can realize the reversible cyclic transition of different states of NGT and SGT under certain conditions. To verify the law accurately, three cyclic tests were respectively carried out for NGT-0.8, NGT-1.0, and NGT-1.6 with the specific parameters listed in Figure S7. As shown in Figure 4D, the reinjected high dielectric water in the

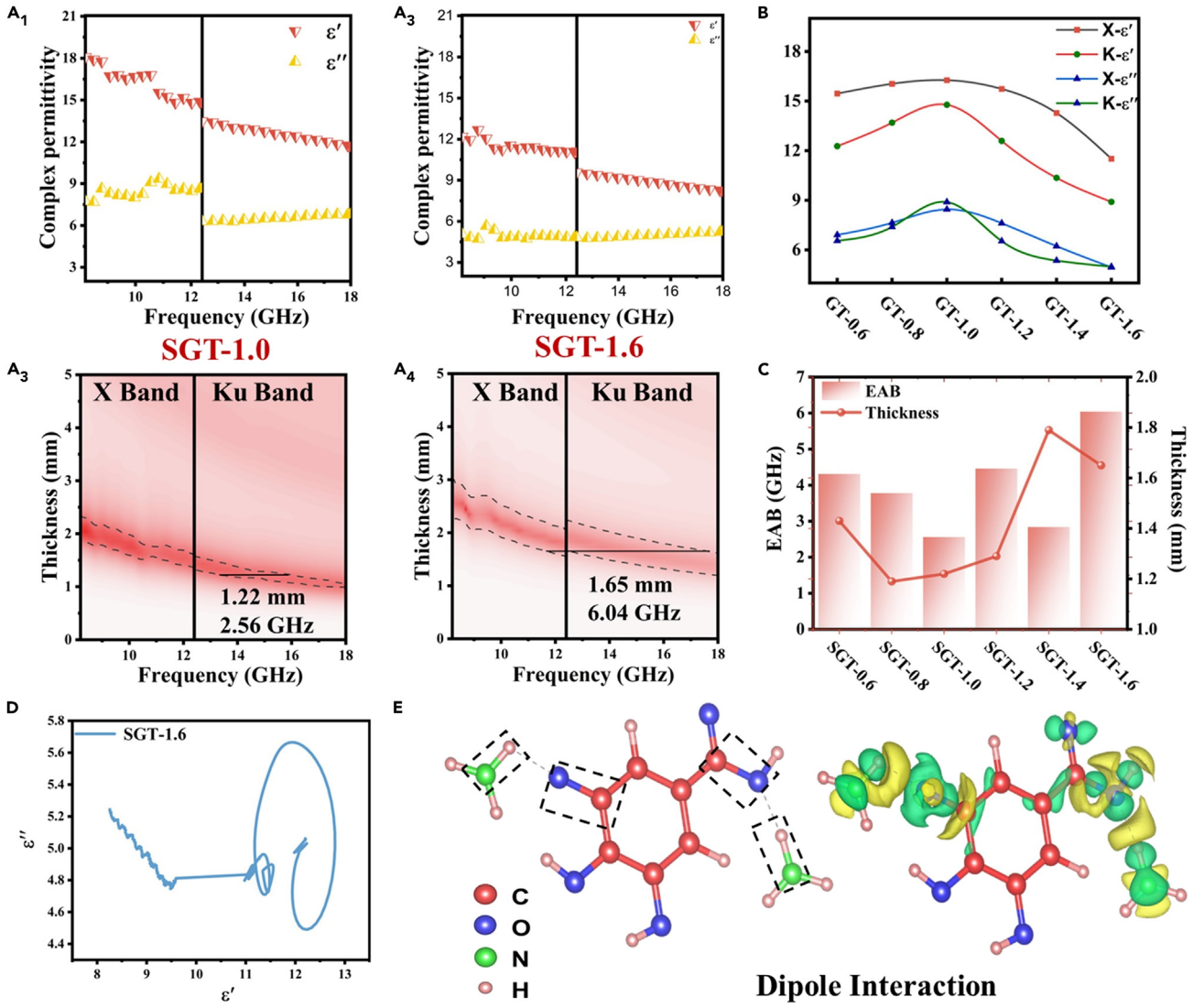

Figure 3. EWA properties and mechanisms of SGT gels

(A_1-A_4) EM parameters of SGT-1.0 and SGT-1.6. See also Figure S1.

(B) EM parameters of SGT gels with different ingredient ratios.

(C) The comparison graph of EWA properties of SGT gels.

(D) *Cole-Cole* semicircle of SGT-1.6 gels. See also Figures S2 and S3.

(E) DFT-based GT gel network models.

gel polymer network contributes to a significantly higher dielectric constant of the SGT state than that of the NGT. And the EM parameters remain almost unchanged in the third recovery compared to the initial NGT. Moreover, three recovery results of the EAB satisfy that NGT is larger than SGT, and the EAB of NGT_3 is larger than that of NGT_2, indicating that the GT gel can still maintain excellent EWA performance after undergoing water-loss and re-recovery process. Successful realization of the S-N-S reversible recovery process enabled GT gels to be adapted to natural conditions in practical applications (Figure 4E). To be specific, various states of NGT and SGT correspond to rainy and sunny days in the natural environment, respectively. On sunny days, the GT gel remains in the NGT state. When it comes to rainy days, the transition from NGT to SGT is realized with rainfall and certain temperatures applied to the NGT. Overall, the state of the GT gel shifts with changing weather, which facilitates further usage of the ECEDs in follow-up.

Multifunctionality application

To achieve flawless FE, the SGT gel necessitates outstanding mechanical prowess (Figure 5A). It adeptly mimics the movements of a human finger, seamlessly bending and folding at any angle. Furthermore, our artificial stretching and compression experiments demonstrated the

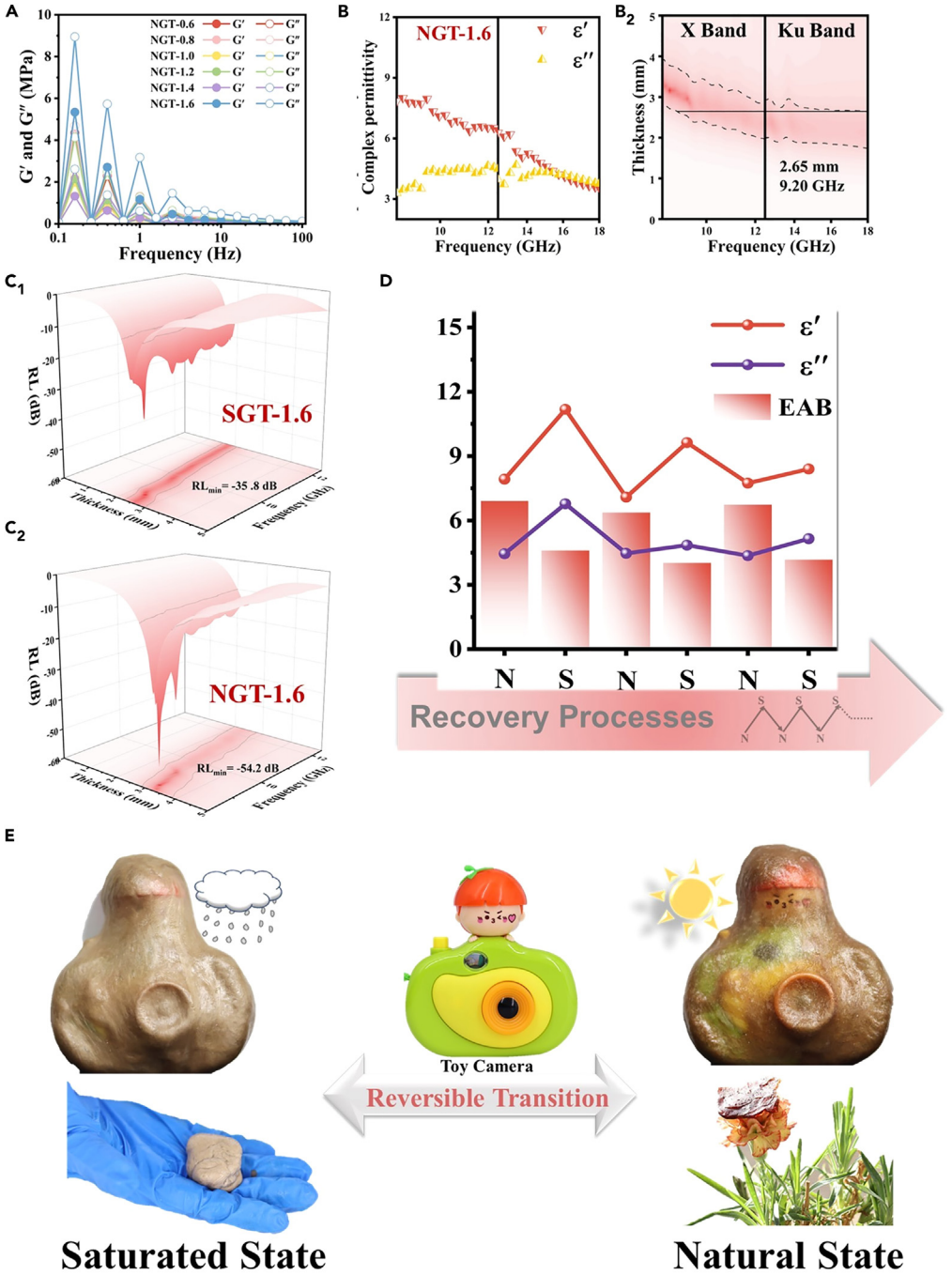

Figure 4. Recovery process between SGT and NGT gels

(A) Rheological characterizations of NGT gels.

(B_1-B_2) EM parameters of NGT-1.6. See also Figures S4 and S5.

(C_1-C_2) 3D RL plots of SGT-1.6 and NGT-1.6. See also Figure S6.

(D) Reversible cyclical process from SGT to NGT (the coordinate axes N-S-N-S-N-S represent the three recovery processes). See also Figure S7.

(E) Use of FE in practical environments.

SGT gel's exceptional capabilities, expanding from a ball to match the length of the experimenter's arm and enduring over 450 g of weight without deformation. Hence, the remarkable flexibility and plasticity of the SGT gel are instrumental in achieving impeccable FE around ECEDs.

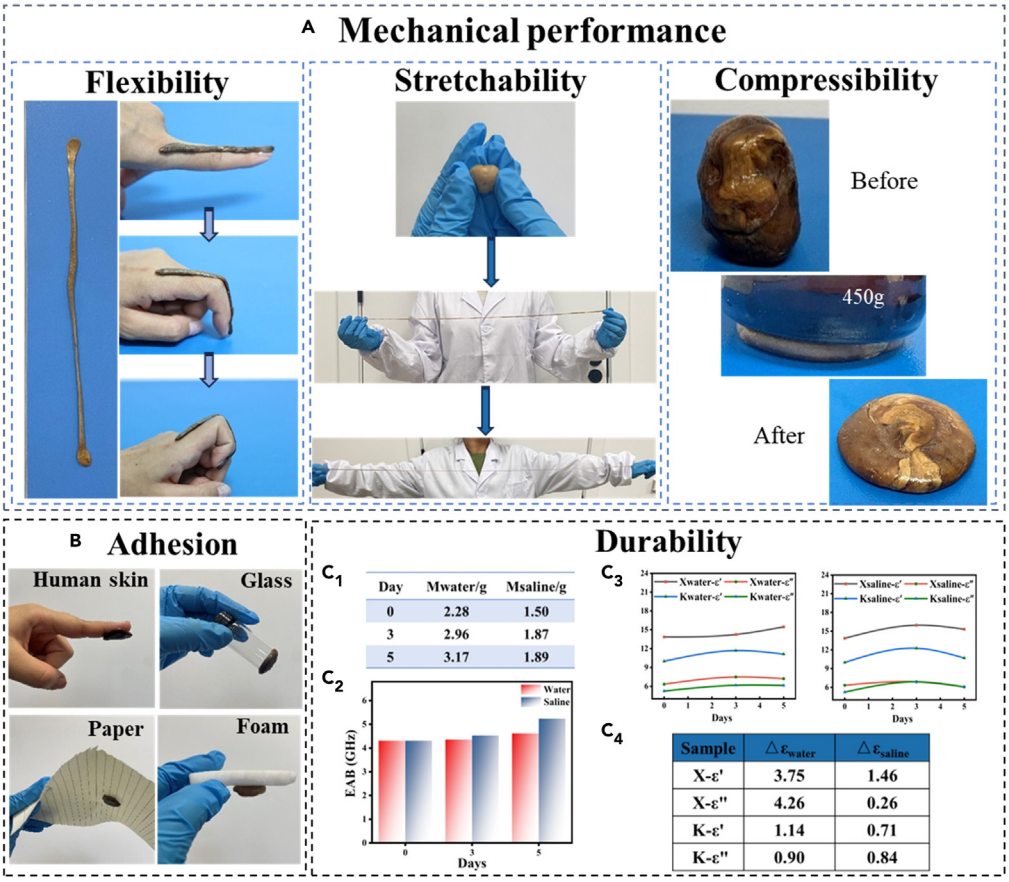

Figure 5. Multifunctionality of GT gels

See also Figures S8–S10.

(A) Mechanical performance of SGT gels.

(B) Adhesion of SGT gels in air.

(C) Durability of GT gels in water and salt water.

The requisite adhesion of SGT serves a vital role in achieving effective FE (Figure 5B). Its ability to adhere to surfaces such as human skin, glass, paper, and other substrates is primarily attributed to the abundant presence of catechol and catechol groups in the molecular structure of tannins.[47] Specifically, SGT gel adhesion mainly originates from hydrogen bonding and intermolecular hydrophobic interactions.[48,49] In summary, the SGT gel, boasting numerous hydrogen bonds, exhibits remarkable deformability and adhesion, enabling adaptation to various shapes and repetitive adhesion to surfaces of diverse objects.

The stability of SGT gel in water and artificial seawater was preliminarily explored, considering potential application environments. To investigate the dissolution behavior, SGT-1.2 was specifically selected, and a 5-day resistance test (Figure 5C) was conducted. It involved dividing the gel into two parts and immersing them, one at room temperature and the other in artificial seawater, for five days, recording observations on days 0, 3, and 5. Remarkably, no discernible corrosion products were observed in the beaker, and the chemical inertness of polymer networks, therefore the SGT gel exhibited stability in solution. Upon contact between the polymer and the solvent, interactions prompt the swelling phenomenon, making the mass of GT-1.2 increase to 1.39 times the initial mass with the increase of the immersion time. Intriguingly, the dielectric parameter of SGT-1.2 remains relatively stable despite the immersion duration (variation range: ε' 0.71–3.75, ε'' 0.26–4.26). Following 5 days of immersion in both water and artificial seawater, the EWA performance of SGT-1.2 surpasses its initial performance. The EAB even reaches 5.24 GHz after the 5-day immersion in seawater, exceeding the original 4.46 GHz, which stems from the effect of the pH of the solution in artificial seawater on the structure of the polymer network.

The SGT gel exhibits physical attributes akin to playdough, showcasing exceptional mechanical strength, robust adhesion, and resistance, facilitating the initial FE of ECEDs (Figure S8) and the gels allow for larger sizes to facilitate process production (Figure S9). In its natural state, the NGT gel exhibits a lighter yet sturdier compared to the original SGT and maintains an effective encapsulating condition. Furthermore, the SGT gel demonstrates appealing thermoplasticity. Sliced into different sizes, it seamlessly consolidates into a unified piece after being exposed to a 50°C oven for 5 min (Figure S10). This favors its swift recyclability in practical application, and favorable recyclability improves the utility of GT gels thus avoiding environmental pollution. We effectively utilize the characteristics of traditional hydrogels that lose water

after placement, GT gels demonstrate outstanding performance across various parameters, encompassing cost-effectiveness, swift and straightforward preparation, user-friendliness, versatile applicability, low energy consumption, and recyclability, which lays a solid foundation for realizing the FE of ECEDs.

Conclusion

In summary, we have successfully developed a versatile, lightweight, and customizable playdough-like EMW absorber GT through the facile chemical cross-linking of polymers and polyphenolic compounds. In the saturated state, SGT-1.6 exhibits exceptional flexibility, plasticity, adhesion, and favorable EWA properties (EAB = 6.04 GHz, Thickness = 1.65 mm), which help to realize the self-encapsulation of ECEDs. When turning to the natural state along with the water loss, NGT-1.6 is lightweight and robust, demonstrating an extensive full-band absorption of 2.8 $\pm$ 0.05 mm within the X-band due to better impedance matching. It exhibits an exceptional EAB of 9.20 GHz, thereby enabling self-optimization of EWA performance. Additionally, the synthesis of GT gel is straightforward and universally applicable, the reversible cyclic transition between SGT and NGT makes the gels more convenient for practical applications. This work provides an effective strategy to overcome the limitations impeding hydrogels as effective EMW absorbers, concurrently broadening the application areas of gelatin-based gels.

Limitations of the study

The EWA properties of the materials were improved by modulating interactions between cross-linkers and raw materials. However, at the microscopic level, due to limitations in characterization techniques, it is difficult to clearly elaborate the mechanism of the interaction between components in the material and EMWs. New methods will be developed in subsequent studies to help us understand the deeper mechanisms more deeply.

STAR★METHODS

Detailed methods are provided in the online version of this paper and include the following:

- KEY RESOURCES TABLE
- RESOURCE AVAILABILITY
  - Lead contact
  - Materials availability
  - Data and code availability
- METHOD DETAILS
  - Materials
  - Synthesis of GT gels
  - Characterization and EM parameter measurement
  - Density functional theory (DFT) calculation

SUPPLEMENTAL INFORMATION

Supplemental information can be found online at https://doi.org/10.1016/j.isci.2024.109725.

ACKNOWLEDGMENTS

Financial support was provided by the National Science Foundation of China (Grants nos. 51872238, 52074227, 21806129, 52362024 and 22004106), the Fundamental Research Funds for the Central Universities (Nos. 3102018zy045 and 3102019AX11), the Natural Science Basic Research Plan in Shaanxi Province of China (Nos. 2017JQ5116 and 2020JM-118), and the Key Laboratory of Icing and Anti/De-icing of CARDC (IADL20220401).

AUTHOR CONTRIBUTIONS

X.Z. designed research, performed experiments, wrote the manuscript; Y.W. and B.S. analyzed data and drew designs; Q.C. analyzed data and reviewed the manuscript; L.Z. designed research, instructed the writing; H.W. designed research, instructed the writing and reviewed the manuscript. All authors discussed the results and contributed to the final manuscript.

DECLARATION OF INTERESTS

The authors declare no competing interests.

Received: February 18, 2024
Revised: April 2, 2024
Accepted: April 8, 2024
Published: April 10, 2024

REFERENCES

1. Liu, H., Li, X., Zhao, X., Zhang, M., Liu, X., Yang, S., Wu, H., and Ma, Z. (2023). Large Annular Dipoles Bounded between Single-Atom Co and Co Cluster for Clarifying Electromagnetic Wave Absorbing Mechanism. Adv. Funct. Mater. *33*, 2304442. https://doi.org/10.1002/adfm.202304442.
2. Wang, C., Lv, Z., Mohan, M.P., Cui, Z., Liu, Z., Jiang, Y., Li, J., Wang, C., Pan, S., Karim, M.F., et al. (2021). Pangolin-Inspired Stretchable, Microwave-Invisible Metascale. Adv. Mater. *33*, 2102131. https://doi.org/10.1002/adma.202102131.
3. Wu, Z., Pei, K., Xing, L., Yu, X., You, W., and Che, R. (2019). Enhanced microwave absorption performance from magnetic coupling of magnetic nanoparticles suspended within hierarchically tubular composite. Adv. Funct. Mater. *29*, 1901448. https://doi.org/10.1002/adfm.201901448.
4. Wang, Q., Li, W., Kang, J., and Wang, Y. (2019). Electromagnetic safety evaluation and protection methods for a wireless charging system in an electric vehicle. IEEE Trans. Electromagn. Compat *61*, 1913–1925. https://doi.org/10.1109/TEMC.2018.2875903.
5. Zhang, C., Shi, Y., Li, X., Wu, H., Shen, Y., Guo, W., Tian, K., and Wang, H. (2022). Architecture inspired structure engineering toward carbon nanotube hybrid for microwave absorption promotion. iScience *25*, 105203. https://doi.org/10.1016/j.isci.2022.105203.
6. Liu, C.W., Chen, M.H., Pi, T.C., Kao, J.C., and Yeh, Y.I. (2022). Demonstration of flexible encapsulation in assembly industry. In 2022 IEEE 72nd Electronic Components and Technology Conference (ECTC) (IEEE), pp. 987–991. https://doi.org/10.1109/ECTC51906.2022.00161.
7. Tian, G., Yang, D., Liang, C., Liu, Y., Chen, J., Zhao, Q., Tang, S., Huang, J., Xu, P., Liu, Z., and Qi, D. (2023). A Nonswelling Hydrogel with Regenerable High Wet Tissue Adhesion for Bioelectronics. Adv. Mater. *35*, e2212302. https://doi.org/10.1002/adma.202212302.
8. Xue, P., Valenzuela, C., Ma, S., Zhang, X., Ma, J., Chen, Y., Xu, X., and Wang, L. (2023). Highly Conductive MXene/PEDOT: PSS-Integrated Poly (N-Isopropylacrylamide) Hydrogels for Bioinspired Somatosensory Soft Actuators. Adv. Funct. Mater. *33*, 2214867. https://doi.org/10.1002/adfm.202214867.
9. Deptula, A., Rangel-Galera, J., and Espinosa-Marzal, R.M. (2023). Control of Surface Morphology, Adhesion and Friction of Colloidal Gels with Lamellar Surface Interactions. Adv. Funct. Mater. *33*, 2300896. https://doi.org/10.1002/adfm.202300896.
10. Wang, G., Liu, Y., Zu, B., Lei, D., Guo, Y., Wang, M., and Dou, X. (2023). Reversible adhesive hydrogel with enhanced sampling efficiency boosted by hydrogen bond and van der Waals force for visualized detection. Chem. Eng. J. *455*, 140493. https://doi.org/10.1016/j.cej.2022.140493.
11. Wang, R., Chen, P., Zhou, X., Sun, L., Wang, G., Liu, Y., and Gao, C. (2023). An Eutectic Gel Based on Polymerizable Deep Eutectic Solvent with Self-Adhesive, Self-adaptive Cold and High Temperature Environments. Adv. Mater. Technol. *8*, 2201509. https://doi.org/10.1002/admt.202201509.
12. Long, Y., Zhang, Z., Sun, K., Wang, C., Zeng, N., Gao, B., Tang, X., Qi, X., and Fan, R. (2023). Enhanced electromagnetic wave absorption performance of hematite@carbon nanotubes/polyacrylamide hydrogel composites with good flexibility and biocompatibility. Adv. Compos. *6*, 173. https://doi.org/10.1007/s42114-023-00749-7.
13. Hu, L., Chee, P.L., Sugiarto, S., Yu, Y., Shi, C., Yan, R., Yao, Z., Shi, X., Zhi, J., Kai, D., et al. (2023). Hydrogel-Based Flexible Electronics. Adv. Mater. *35*, 2205326. https://doi.org/10.1002/adma.202205326.
14. Li, T., Wei, H., Zhang, Y., Wan, T., Cui, D., Zhao, S., Zhang, T., Ji, Y., Algadi, H., Guo, Z., et al. (2023). Sodium alginate reinforced polyacrylamide/xanthan gum double network ionic hydrogels for stress sensing and self-powered wearable device applications. Carbohydr. Polym. *309*, 120678. https://doi.org/10.1016/j.carbpol.2023.120678.
15. Meazza, L., Foster, J.A., Fucke, K., Metrangolo, P., Resnati, G., and Steed, J.W. (2013). Halogen-bonding-triggered supramolecular gel formation. Nat. Chem. *5*, 42–47. https://doi.org/10.1038/NCHEM.1496.
16. Pena-Francesch, A., Jung, H., Demirel, M.C., and Sitti, M. (2020). Biosynthetic self-healing materials for soft machines. Nat. Mater. *19*, 1230–1235. https://doi.org/10.1038/s41563-020-0736-2.
17. Kandambeth, S., Shinde, D.B., Panda, M.K., Lukose, B., Heine, T., and Banerjee, R. (2013). Enhancement of Chemical Stability and Crystallinity in Porphyrin-Containing Covalent Organic Frameworks by Intramolecular Hydrogen Bonds. Angew. Chem. *52*, 13052–13056. https://doi.org/10.1002/anie.201306775.
18. Lai, J.-C., Mei, J.-F., Jia, X.-Y., Li, C.-H., You, X.-Z., and Bao, Z. (2016). A Stiff and Healable Polymer Based on Dynamic-Covalent Boroxine Bonds. Adv. Mater. *28*, 8277–8282. https://doi.org/10.1002/adma.201602332.
19. Ying, H., Zhang, Y., and Cheng, J. (2014). Dynamic urea bond for the design of reversible and self-healing polymers. Nat. Commun. *5*, 3218. https://doi.org/10.1038/ncomms4218.
20. Alipal, J., Mohd Pu'ad, N., Lee, T.C., Nayan, N.H.M., Sahari, N., Basri, H., Idris, M.I., and Abdullah, H.Z. (2021). A review of gelatin: Properties, sources, process, applications, and commercialisation. Mater. Today: Proc. *42*, 240–250. https://doi.org/10.1016/j.matpr.2020.12.922.
21. Andreazza, R., Morales, A., Pieniz, S., and Labidi, J. (2023). Gelatin-Based Hydrogels: Potential Biomaterials for Remediation. Polymers *15*, 1026. https://doi.org/10.3390/polym15041026.
22. Huang, T., Tu, Z.C., Shangguan, X., Sha, X., Wang, H., Zhang, L., and Bansal, N. (2019). Fish gelatin modifications: A comprehensive review. Trends Food Sci. Technol. *86*, 260–269. https://doi.org/10.1016/j.tifs.2019.02.048.
23. Kim, D., Yoo, H., Kim, K., Kim, D., Kim, K.T., Kim, C., Kim, J.Y., Moon, H.R., and Kim, M. (2022). Post-synthetic ligand cyclization in metal-organic frameworks through functional group connection with regioisomerism. Chem. Commun. *58*, 5948–5951. https://doi.org/10.1039/d2cc01031c.
24. Qin, P., Zhang, C., Guo, Y., Zhang, D., Liu, Q., Li, Y., Song, H., and Lv, Z. (2024). Hydroxyl and amino dual-functionalized core-shell molecular sieves featuring hydrogen bond donor groups for efficient CO_2 cycloaddition. J. Colloid Interface Sci. *656*, 68–79. https://doi.org/10.1016/j.jcis.2023.11.088.
25. Dankar, I., Haddarah, A., Omar, F.E.L., Pujolà, M., and Sepulcre, F. (2018). Characterization of food additive-potato starch complexes by FTIR and X-ray diffraction. Food Chem. *260*, 7–12. https://doi.org/10.1016/j.foodchem.2018.03.138.
26. Muhoza, B., Xia, S., and Zhang, X. (2019). Gelatin and high methyl pectin coacervates crosslinked with tannic acid: The characterization, rheological properties, and application for peppermint oil microencapsulation. Food Hydrocoll. *97*, 105174. https://doi.org/10.1016/j.foodhyd.2019.105174.
27. Abidi, N., Cabrales, L., and Haigler, C.H. (2014). Changes in the cell wall and cellulose content of developing cotton fibers investigated by FTIR spectroscopy. Carbohydr. Polym. *100*, 9–16. https://doi.org/10.1016/j.carbpol.2013.01.074.
28. Warren, F.J., Gidley, M.J., and Flanagan, B.M. (2016). Infrared spectroscopy as a tool to characterise starch ordered structure-a joint FTIR-ATR, NMR, XRD and DSC study. Carbohydr. Polym. *139*, 35–42. https://doi.org/10.1016/j.carbpol.2015.11.066.
29. Godiya, C.B., Kumar, S., and Xiao, Y. (2020). Amine functionalized egg albumin hydrogel with enhanced adsorption potential for diclofenac sodium in water. J. Hazard Mater. *393*, 122417. https://doi.org/10.1016/j.jhazmat.2020.122417.
30. Zeng, H., Yu, Z., Shao, L., Li, X., Zhu, M., Liu, Y., Feng, X., and Zhu, X. (2021). A novel strategy for enhancing the performance of membranes for dyes separation: Embedding PAA@ UiO-66-NH_2 between graphene oxide sheets. Chem. Eng. J. *403*, 126281. https://doi.org/10.1016/j.cej.2020.126281.
31. Fang, L., Zhang, C., Ge, W., Rong, M., Chen, F., Chen, Z., Wang, X., Zheng, Z., and Huang, Q. (2023). Facile spinning of tough and conductive eutectogel fibers via Li+-induced dense hydrogen-bond networks. Chem. Eng. J. *478*, 147405. https://doi.org/10.1016/j.cej.2023.147405.
32. Song, J., Chen, S., Sun, L., Guo, Y., Zhang, L., Wang, S., Xuan, H., Guan, Q., and You, Z. (2020). Mechanically and electronically robust transparent organohydrogel fibers. Adv. Mater. *32*, 1906994. https://doi.org/10.1002/adma.201906994.
33. Li, W., Xu, M., Xu, H.X., Wang, X., and Huang, W. (2022). Metamaterial absorbers: From tunable surface to structural transformation. Adv. Mater. *34*, 2202509. https://doi.org/10.1002/adma.202202509.
34. Yao, P., Bao, Q., Yao, Y., Xiao, M., Xu, Z., Yang, J., and Liu, W. (2023). Environmentally Stable, Robust, Adhesive, and Conductive Supramolecular Deep Eutectic Gels as Ultrasensitive Flexible Temperature Sensor. Adv. Mater. *35*, e2300114. https://doi.org/10.1002/adma.202300114.
35. Stojkov, G., Niyazov, Z., Picchioni, F., and Bose, R.K. (2021). Relationship between Structure and Rheology of Hydrogels for Various Applications. Gels *7*, 255. https://doi.org/10.3390/gels7040255.
36. Yang, Y., Liang, Y., Chen, J., Duan, X., and Guo, B. (2022). Mussel-inspired adhesive antioxidant antibacterial hemostatic composite hydrogel wound dressing via

photo-polymerization for infected skin wound healing. Bioact. Mater. *8*, 341–354. https://doi.org/10.1016/j.bioactmat.2021.06.014.

37. Hui, S., Zhang, L., and Wu, H. (2023). Cationic doping induced sulfur vacancy formation in polyionic sulfide for enhanced electromagnetic wave absorption. J. Colloid Interface Sci. *629*, 147–155. https://doi.org/10.1016/j.jcis.2022.09.078.
38. Zhu, H., Jiao, Q., Fu, R., Su, P., Yang, C., Feng, C., Li, H., Shi, D., and Zhao, Y. (2022). Cu/NC@Co/NC composites derived from core-shell Cu-MOF@Co-MOF and their electromagnetic wave absorption properties. J. Colloid Interface Sci. *613*, 182–193. https://doi.org/10.1016/j.jcis.2021.11.166.
39. Qin, M., Zhang, L., and Wu, H. (2022). Dielectric Loss Mechanism in Electromagnetic Wave Absorbing Materials. Adv. Sci. *9*, 2105553. https://doi.org/10.1002/advs.202105553.
40. Liu, H., Liu, R., Chen, K., Liu, Y., Zhao, Y., Cui, X., and Tian, Y. (2023). Bioinspired gradient structured soft actuators: From fabrication to application. Chem. Eng. J. *461*, 141966. https://doi.org/10.1016/j.cej.2023.141966.
41. Chen, Y., Yi, X., Zhang, Z., Ding, B., Li, Z., and Luo, Y. (2022). High internal phase Pickering emulsions stabilized by tannic acid-ovalbumin complexes: Interfacial property and stability. Food Hydrocoll. *125*, 107332. https://doi.org/10.1016/j.foodhyd.2021.107332.
42. Armstrong, C.E.J., Gilmore, A.M., Boss, P.K., Pagay, V., and Jeffery, D.W. (2023). Machine learning for classifying and predicting grape maturity indices using absorbance and fluorescence spectra. Food Chem. *403*, 134321. https://doi.org/10.1016/j.foodchem.2022.134321.
43. Ma, M., Zhong, Y., and Jiang, X. (2020). Thermosensitive and pH-responsive tannin-containing hydroxypropyl chitin hydrogel with long-lasting antibacterial activity for wound healing. Carbohydr. Polym. *236*, 116096. https://doi.org/10.1016/j.carbpol.2020.116096.
44. Han, Z., Wang, P., Lu, Y., Jia, Z., Qu, S., and Yang, W. (2022). A versatile hydrogel network-repairing strategy achieved by the covalent-like hydrogen bond interaction. Sci. Adv. *8*, eabl5066. https://doi.org/10.1126/sciadv.abl5066.
45. Li, Y., Sui, J., Cui, L.-S., and Jiang, H.-L. (2023). Hydrogen Bonding Regulated Flexibility and Disorder in Hydrazone- Linked Covalent Organic Frameworks. J. Am. Chem. Soc. *145*, 1359–1366. https://doi.org/10.1021/jacs.2c11926.
46. Cofelice, M., Messia, M.C., Marconi, E., Cuomo, F., and Lopez, F. (2023). Effect of the xanthan gum on the rheological properties of alginate hydrogels. Food Hydrocoll. *142*, 108768. https://doi.org/10.1016/j.foodhyd.2023.108768.
47. Yin, J., Pan, S., Wu, L., Tan, L., Chen, D., Huang, S., Zhang, Y., and He, P. (2020). A self-adhesive wearable strain sensor based on a highly stretchable, tough, self-healing and ultra-sensitive ionic hydrogel. J. Mater. *8*, 17349–17364. https://doi.org/10.1039/d0tc04144k.
48. Zhao, L., Ren, Z., Liu, X., Ling, Q., Li, Z., and Gu, H. (2021). A Multifunctional, Self-Healing, Self-Adhesive, and Conductive Sodium Alginate/Poly (vinyl alcohol) Composite Hydrogel as a Flexible Strain Sensor. ACS Appl. Mater. Inter. *13*, 11344–11355. https://doi.org/10.1021/acsami.1c01343.
49. Ling, Q., Fan, X., Ling, M., Liu, J., Zhao, L., and Gu, H. (2023). Collagen-based organohydrogel strain sensor with self-healing and adhesive properties for detecting human motion. ACS Appl. Mater. Inter. *15*, 12350–12362. https://doi.org/10.1021/acsami.2c21566.

STAR★METHODS

KEY RESOURCES TABLE

REAGENT or RESOURCE	SOURCE	IDENTIFIER
Chemicals, peptides, and recombinant proteins		
Gelatin (Gum intensity 250g bloom, 100g)	Macklin	CAS: 9000-70-8
Tannin acid (AR, 98%)	Rhawn	CAS: 1401-55-4
Deposited data		
All data reported in this paper will be shared by the lead contact upon request.		

RESOURCE AVAILABILITY

Lead contact

Further information and requests for resources and reagents should be directed to and will be fulfilled by the Lead Contact, Hongjing Wu (wuhongjing@nwpu.edu.cn).

Materials availability

This study did not generate new unique reagents.

Data and code availability

All data reported in this paper will be shared by the lead contact upon request. This paper does not report original code. Any additional information required to reanalyze the data reported in this paper is available from the lead contact upon request.

METHOD DETAILS

Materials

Gelatin (gum intensity 250g) and tannin acid (AR) were purchased from Macklin and Rhawn, respectively. All reagents in this work are analytical purity and utilized directly without further purification.

Synthesis of GT gels

The preparation process is shown in Figure 1. Specifically, First, gelatin solution with a concentration of 0.383 mol L^{-1} and tannic acid solution with a concentration of 0.118 mol L^{-1} were configured, respectively. Second, tannic acid was mixed into the gelatin solution and stirred at 60°C for 5 min, after which the supernatant was poured off to obtain the SGT gel. We prepared six samples with gelatin to tannic acid mass ratios of 1.0:0.6, 1.0:0.8, 1.0:1.0, 1.0:1.2, 1.0:1.4; 1.0:1.6, respectively.

Characterization and EM parameter measurement

Scanning electron microscope images were obtained using ZEISS MERLIN electron microscopy. The chemical structures of GT gels were characterized by attenuated total reflection Fourier transform infrared spectroscopy (ATR-FTIR) and X-ray photoelectron spectroscopy (Kratos AXIS Ultra DLD). The thermal properties of GT gels were tested using a Differential Scanning Calorimeter (DSC) model DSC214 (made in Germany) and a Thermogravimetric Analyzer (TGA) model TGA8000 (PerkinElmer, U.S.A.) The temperature intervals of the DSC and the TGA were set at 5-100°C and 30-250°C, respectively. Dynamic rheological testing was performed over a frequency range of 0.1 to 100 Hz (0.628-628 rad/s) using an MCR 302 rheometer (DHR-3, TA).

The WR-90 coaxial rectangular waveguide fixture was used to test electromagnetic parameters in the X- and KU-band frequency ranges. Specific equipment included an Anritsu MS46322B vector network analyzer and BJ100 and BJ140 coaxial waveguide adapters. The WR-90 test fixture used samples with dimensions of 22.86 mm × 10.16 mm, and the WR-62 test fixture (12.4 to 18.0 GHz) samples with internal dimensions of 15.79 mm × 7.89 mm. All samples are precisely cut to standard dimensions.

Density functional theory (DFT) calculation

Density of states calculations of the samples are performed utilizing the Vienna Ab initio Simulation Package (VASP) based on density flood theory (DFT). The exchange and correlations were dealt with the Perdew-Burke Ernzerhof (PBE) functional within the Generalized Gradient Approximation (GGA) framework. The Brillourin zone was sampled with Monkhorst K-point mesh 3 × 2 × 1 through all the computational process. In the differential charge density calculation process, the structures were geometrically optimized and considered as converged with the energy tolerance less than 10^{-5} eV, iterative calculation using conjugate gradient method.